

Article

Effect of Al₂O₃ on Sintering Reaction of Calcium Ferrite

Zhenwei Jing¹, Xiaofei Xing², Hongyan Yan^{1,*}, Ju Meng¹, Xiwei Qi¹, Hui Li¹ and Jinglong Liang¹

¹ College of Metallurgy and Energy, North China University of Science and Technology, Tangshan 063210, China

² Tangshan Research Institute, Beijing Institute of Technology, Tangshan 063004, China

* Correspondence: yanhy@ncst.edu.cn

Abstract: Calcium ferrite containing aluminum (CFA) has been widely used in blast furnace production because it is an important compound that affects the quality of sinter. The influence of Al₂O₃ on CFA preparation process was studied by the raw material of CaO-Fe₂O₃-Al₂O₃. Diffraction of x-rays (XRD), scanning electron microscope (SEM) and electrochemical impedance spectroscopy (EIS) analysis were used to analyze the phase, micro morphology and the reducibility of the products. The results showed that CaO tended to combine more with Fe₂O₃ to form calcium ferrite with the increase of Fe₂O₃, whereas CaO tended to combine more with Al₂O₃ to form calcium aluminate with the content of Al₂O₃ above 45%. The micro morphology of sintered samples had a stable sintering skeleton structure due to the existence of calcium ferrite. Calcium ferrite was distributed between different particles in flakes, whereas calcium aluminate was attached to the Al₂O₃ particle surface. The large amount of calcium aluminate inhibited the emergence of calcium ferrite, and it had an adverse impact on the reducibility of sinter and the preparation of CFA.

Keywords: calcium ferrite; calcium aluminate; Al₂O₃ content; sintering



Citation: Jing, Z.; Xing, X.; Yan, H.; Meng, J.; Qi, X.; Li, H.; Liang, J. Effect of Al₂O₃ on Sintering Reaction of Calcium Ferrite. *Crystals* **2022**, *12*, 1172. <https://doi.org/10.3390/cryst12081172>

Academic Editor: Vladislav V. Khartov

Received: 5 August 2022

Accepted: 18 August 2022

Published: 20 August 2022

Publisher's Note: MDPI stays neutral with regard to jurisdictional claims in published maps and institutional affiliations.



Copyright: © 2022 by the authors. Licensee MDPI, Basel, Switzerland. This article is an open access article distributed under the terms and conditions of the Creative Commons Attribution (CC BY) license (<https://creativecommons.org/licenses/by/4.0/>).

1. Introduction

Sinter is sintered by powder ore and flux ingredients, and the quality of sinter directly affects the smooth production of blast furnace ironmaking [1,2]. Sinter requires characteristics of stable composition, high strength and good reducibility. The fundamental reason for the above characteristics is the formation of the binder phase calcium ferrite [3]. Calcium ferrite has been used in the production of blast furnace as a flux type sinter since 1930s [4]. There is little pure calcium ferrite in minerals, and the mineral phases containing magnesium, aluminum and silicon in the vein components. These oxides solidly dissolve into calcium ferrite during the sintering process, form calcium ferrite containing aluminum (CFA) and then transform into multi-component composite calcium ferrite (SFCA) [5,6]. SFCA is a low melting point binder phase mineral with high strength and good reducibility in sintered ore. Its Al₂O₃ composition is an important factor that affects the microstructure and macroscopic quality of sinter [7–10]. The stability of SFCA in sinter depends on the content of Al₂O₃ [11]. SFCA can stably exist with the mass fraction of Al₂O₃ exceeding 2.5%, otherwise, it will decompose into silicate and magnetite. Machida [12] found that the increase of alkalinity caused by Al₂O₃ promoted the formation of calcium ferrite at low temperatures, resulting in the appearance of pores in the sinter and the decrease of strength. CFA is a very important intermediate compound in the transition from calcium ferrite to SFCA, and the influence of Al₂O₃ content on its preparation process is worth studying. However, previous studies mainly focused on the range of low Al₂O₃ mass fraction (less than 20%), and the influence of using high Al₂O₃ mass fraction (more than 20%) to prepare sinter is not clear [13–16]. In order to provide more references for the preparation of CFA and the application of high-alumina sinter, it is necessary to study the influence of high Al₂O₃ ratio on the sintering process of calcium ferrite.

In this paper, Fe₂O₃, Al₂O₃ and CaO powder was used as raw material. The content of Al₂O₃ was 18%, 36%, 45% and 60% was used to sinter at 80 °C. The effect of alumina content on the phase and morphology of sintered products was characterized by XRD and SEM. The influence of the reducibility of the sintered material was analyzed by electrochemical impedance spectroscopy (EIS).

2. Experimental Section

The raw materials were Fe₂O₃, Al₂O₃ and CaO powders with a purity of 99.9%, produced by Shanghai Sinopharm. The average particle sizes of Fe₂O₃, Al₂O₃ and CaO were 2 μm, 8 μm and 3 μm, respectively. In order to prevent CaO from absorbing water, these powders were dried for 6 h at 200 °C, respectively. The raw material mass ratios of the four sintered samples were shown in Table 1. The CaO content selected in this experiment was fixed at 10%. The CaO content in steel making sinter is mostly between 8% and 14%. CaO will affect the basicity of sinter, and when the basicity increases, it is good for the strength of sinter, but it will affect the grade of sinter and reduce the smelting strength of the blast furnace. This CaO content is suitable for the needs of the blast furnace burden structure of steel plants. The powders were weighed and mixed, then XQM-2 vertical (Tencan Powder, Changsha, China) planetary for ball milling was used. Absolute ethanol was used as the dispersion medium, ball milling speed was 300 r/min and milling time was 6 h. After ball milling, the samples were placed in a DZF-6050 vacuum drying oven at 120 °C for 30 min. After drying, the powder mixture was pressed into cylindrical pellets (15 × 3 × 1 mm³) under a uniaxial pressure of 6 MPa for 3 min. Then, the pellets were put into a tubular furnace (BLMT-GB17810) (Bolemant Electric Furnace, Luoyang, China) to sinter at 800 °C for 5 h, with the heating rate of the furnace at 5 °C·min⁻¹.

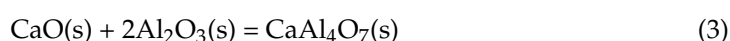
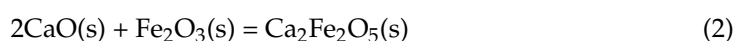
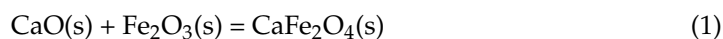
Table 1. Experimental conditions (Mass fraction, %).

Samples	CaO	Fe ₂ O ₃	Al ₂ O ₃
S1	10	30	60
S2	10	45	45
S3	10	54	36
S4	10	72	18

The cooled samples were characterized by using X-ray diffraction (PANalytical, Amelo, Netherlands). The angle of X-ray diffraction is 5° to 90°, and the scanning speed is 10°/min. The acceleration voltage of the electron microscope is 5.0 kV. The microstructure and element analyses were carried out with SEM and EDS (Zeiss, Oberkochen, Germany). The electrochemical workstation (Chinstruments, Shanghai, China) was used to test the electrochemical impedance spectroscopy of the pellets to analyze the reduction differences caused by different ingredients. High frequency was set to 10⁶ Hz, and low frequency was set to 0.1 Hz. Scanning rate was 10 mV/s.

3. Results and Discussion

Thermodynamic calculation was analyzed by using Factsage7.3 software (Aachen, Germany), shown in Figure 1. Fe₂O₃ and Al₂O₃ will not react in theory, and there is almost no solid solution reaction [17]. The reaction in the sintering process is mainly on the Al₂O₃-CaO and Fe₂O₃-CaO systems, shown in Equations (1)–(4). CaO spontaneously reacted with Fe₂O₃ and Al₂O₃ to form calcium ferrite and calcium aluminate at 800 °C. Ca₂Fe₂O₅ was formed before calcium aluminate (CaAl₄O₇, CaAl₂O₄), and CaFe₂O₄ was finally formed.



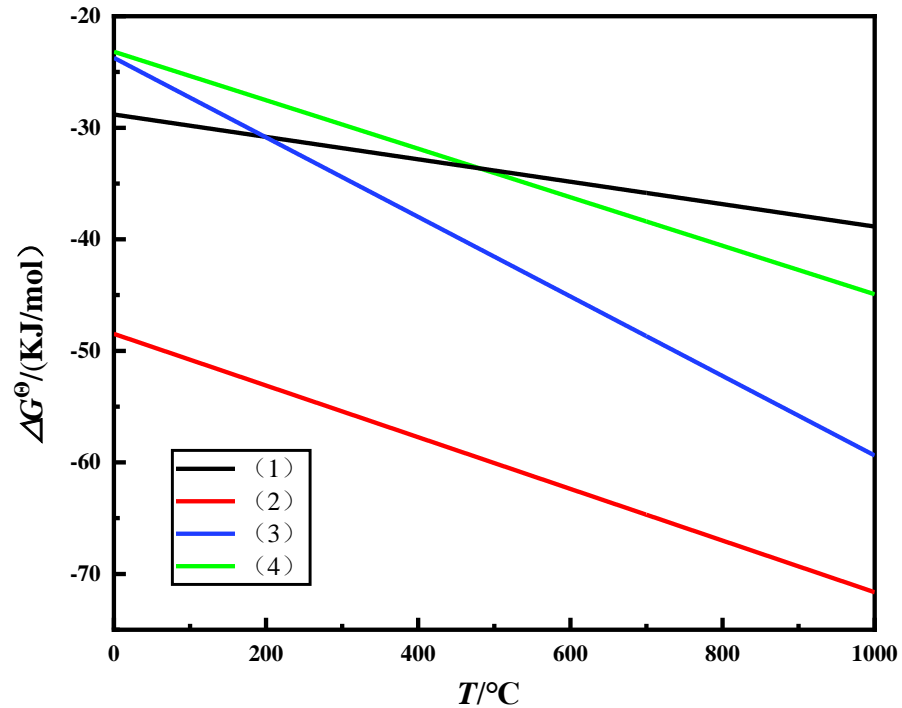
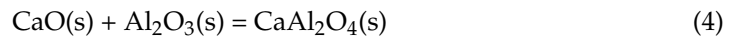


Figure 1. Calculation results of standard Gibbs free energy of chemical reaction at temperature of 0~1000 °C.

Figure 2 shows the XRD patterns of samples in different Al_2O_3 - Fe_2O_3 mass ratios. The content of Al_2O_3 decreased sequentially from S1 to S4. S1 obtained CaAl_2O_4 by Reaction (4). S2 obtained $\text{Ca}_2\text{Fe}_2\text{O}_5$ and CaAl_2O_4 by Reactions (2) and (4). S3 obtained $\text{Ca}_2\text{Fe}_2\text{O}_5$ by Reaction (2). The form of calcium ferrite in sample S4 was CaFe_2O_4 , and due to the formed $\text{Ca}_2\text{Fe}_2\text{O}_5$ can react with excessive Fe_2O_3 to form CaFe_2O_4 [18]. With the decrease of Al_2O_3 content, calcium aluminate gradually disappeared, and calcium ferrite changed from $\text{Ca}_2\text{Fe}_2\text{O}_5$ to CaFe_2O_4 . The reason was that reaction rate of the elementary reaction was proportional to the product of the power of the concentration of each reactant by the law of mass action [19]. The reaction rate of excessive Al_2O_3 was higher than that of Fe_2O_3 with a less amount, and CaO preferentially reacted with Al_2O_3 to produce CaAl_2O_4 . As the Al_2O_3 content decreased, the influence of the law of mass action decreased gradually, and the reaction followed the laws of thermodynamics. The standard Gibbs free energy generated by $\text{Ca}_2\text{Fe}_2\text{O}_5$ was less than CaAl_2O_4 , the content of Al_2O_3 , Fe_2O_3 was same, and the law of mass action is comparable to the effect of thermodynamics on reactions, $\text{Ca}_2\text{Fe}_2\text{O}_5$ and CaAl_2O_4 coexisted in the sample S2. As the mass proportion of Fe_2O_3 further increased, there was no calcium aluminate in sample S3 and sample S4. On the one hand, when the content of Fe_2O_3 was more than Al_2O_3 , the probability of collision between Fe_2O_3 particles and CaO particles was greater, and the quantity of activated molecules became more, and CaO reacted with Fe_2O_3 preferentially. On the other hand, the size of Al_2O_3 was significantly larger than Fe_2O_3 , Fe_2O_3 and had a larger specific surface area than Al_2O_3 . Therefore, the contact surface areas between CaO and Fe_2O_3 were larger, and the formation of calcium ferrite was more favorable. The kinetic conditions for the formation of the calcium iron oxide phase were better than those for the formation of the calcium aluminum oxide phase.

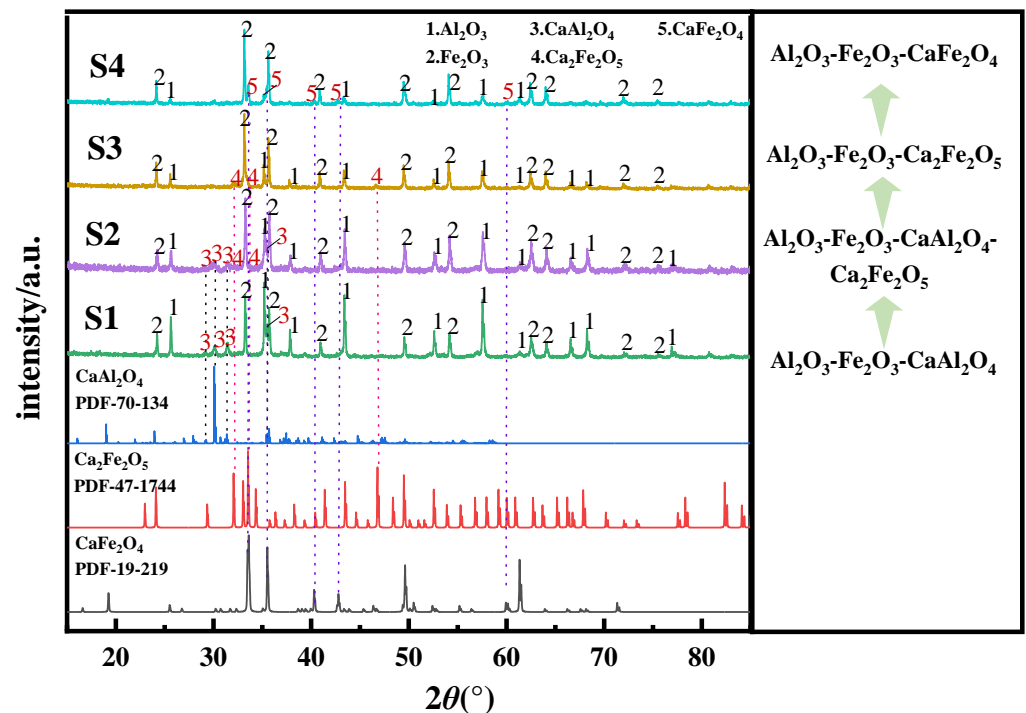


Figure 2. XRD images of different proportion of pellets sintered at 800 °C for 5 h.

Figure 3 showed the SEM images of samples. The contact between different particles of the sintered sample was closer than that before sintering, and a stable sintering skeleton structure was formed. With the increase of Fe_2O_3 content, the number of pores in sintered samples decreased [20]. The smaller Fe_2O_3 particles can more fully fill the pores in the structure. In addition, the generated calcium ferrite had a bonding effect, the overall structure was more compact, and the contact among particles was better. Figure 4 was the SEM and energy spectrum point scan analysis of sample S3. It determined that particles with a smaller size were Fe_2O_3 at 003 point. These particles were densely and evenly distributed in the sample. The larger particles were Al_2O_3 according to the 001 point. The particles as chunk form or pellet form were calcium ferrite particles produced by sintering according to 002 in Figure 4, and they were evenly distributed between Fe_2O_3 and Al_2O_3 particles. Figure 5 showed the SEM and EDS surface scan images of sample S3. The main distribution position of Ca element was the same as that of the Fe element. Combined with the results of Figures 2, 4 and 5, it indicated that the particles in chunk form or pellet form were $\text{Ca}_2\text{Fe}_2\text{O}_5$ particles. $\text{Ca}_2\text{Fe}_2\text{O}_5$ and Fe_2O_3 particles were dispersed in the whole sample and closely contacted Al_2O_3 particles and formed a relatively dense structure.

Figure 6 showed the SEM images of samples S1–S4 with higher magnification. CaAl_2O_4 was formed by the reaction of adjacent CaO and Al_2O_3 particles, and it grew on larger Al_2O_3 particles in the microstructure. Combined with the XRD analysis of S1 and S2 in Figure 2, it was determined that the unique particle that formed the dendritic and leafy morphology in Figure 6a was CaAl_2O_4 . According to Figure 4, the strip-shaped or needle-shaped particles interspersed between Al_2O_3 and Fe_2O_3 in Figure 6b–d was calcium ferrite. The $\text{Al}_2\text{O}_3/\text{Fe}_2\text{O}_3/\text{Ca}_2\text{Fe}_2\text{O}_5/\text{CaAl}_2\text{O}_4$ solid interface appeared in Figure 6b. According to the XRD results, the calcium ferrite in Figure 6d was CaFe_2O_4 , and its needle structure was less obvious than that of $\text{Ca}_2\text{Fe}_2\text{O}_5$ in Figure 6c.

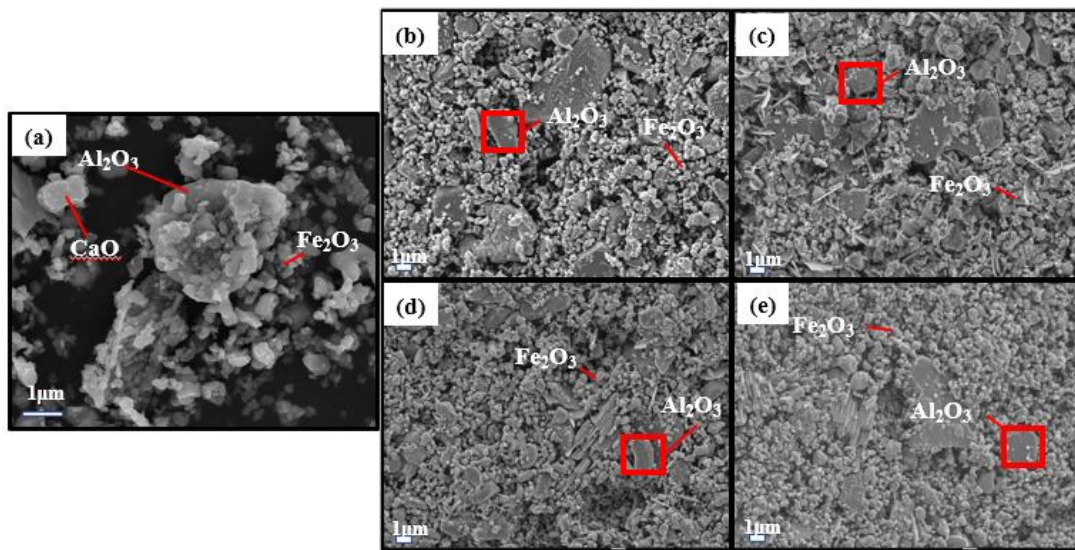


Figure 3. The SEM image of the raw material before sintering in (a) and the SEM images of S1 in (b), S2 in (c), S3 in (d) and S4 in (e).

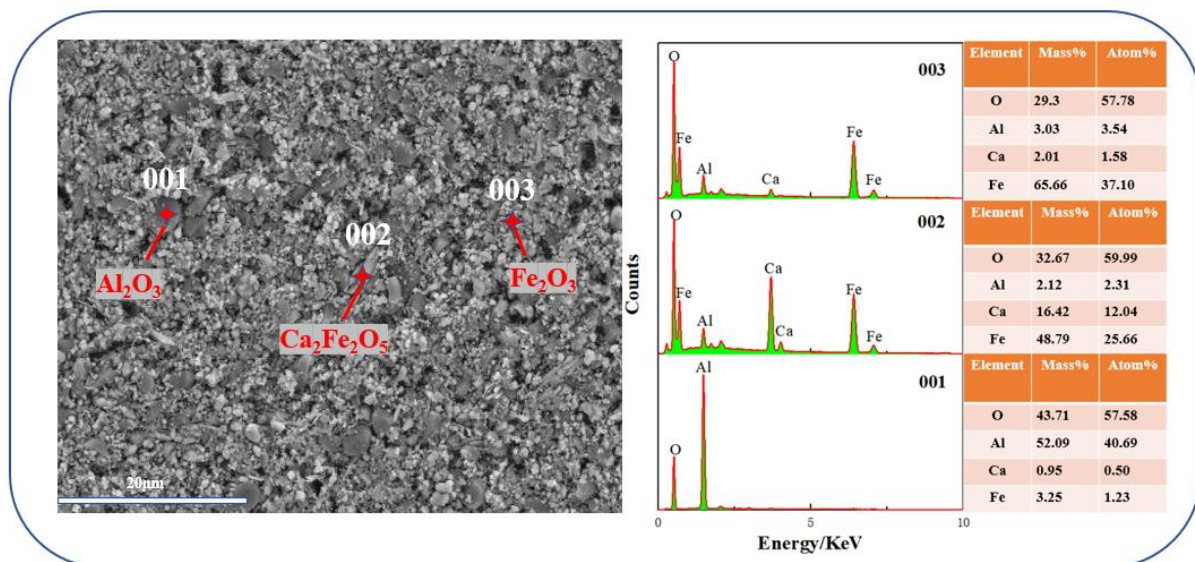


Figure 4. SEM and energy spectrum point scan analysis of sample S3.

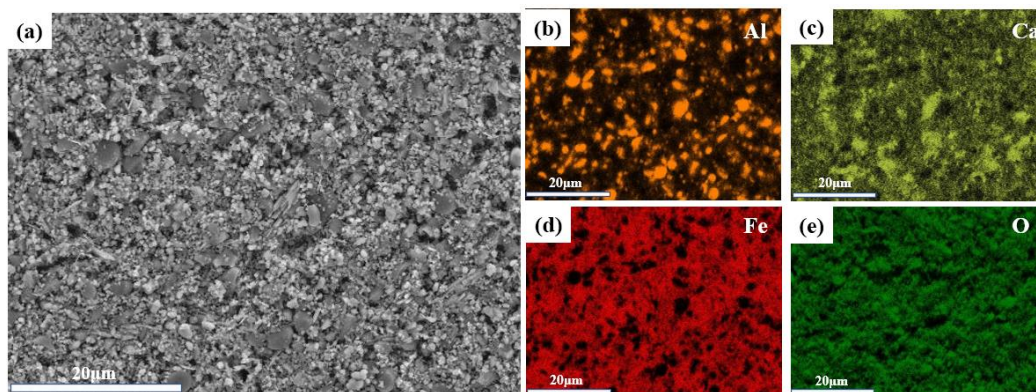


Figure 5. The SEM images of S3 in (a), EDS spectrum of Al in (b), EDS spectrum of Ca in (c), EDS spectrum of Fe in (d) and the EDS spectrum of O in (e).

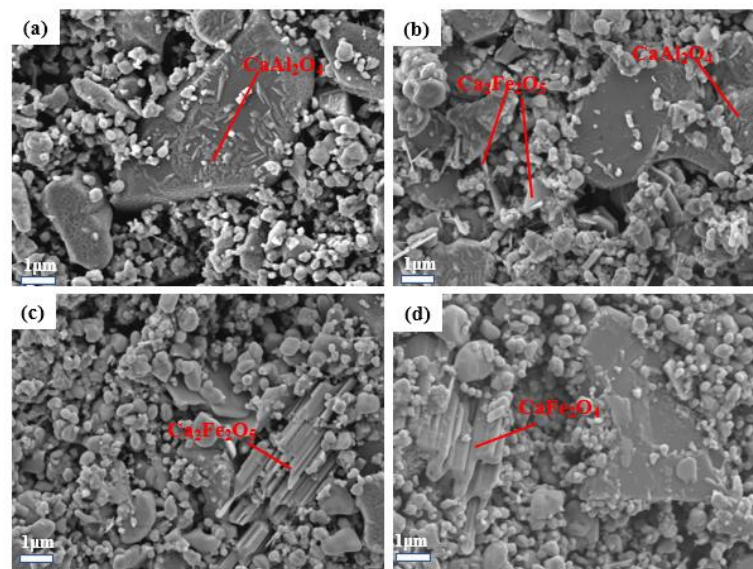


Figure 6. SEM images with higher magnification of sample S1 in (a), sample S2 in (b), sample S3 in (c) and sample S4 in (d).

As a sinter, the reducibility of calcium ferrite is key property, and the reduction process is actually the process of electron loss. The reducibility is stronger, and the ability of electron loss is stronger. The reducibility can be expressed as its resistance. Figure 7 showed the electrochemical impedance spectroscopy (EIS) analysis diagram of samples S1~S4. In the equivalent circuit of the analysis diagram, RS (Ω) represented the solution resistance, RCT represented the charge transfer resistance, ZW was the diffusion impedance and $C1$ represented the capacitive element in the electrochemical measurement device. The Nyquist curve in the figure was composed of the high-frequency circular arc in the first half and the low-frequency line in the second half. The radius or area of the circular arc in the high-frequency area reflected the size of RCT , and it represented the internal resistance of the pellet. When the internal resistance was smaller, the radius of the circular arc was smaller. The order of arc radius in high frequency region was $S1 > S2 > S3 > S4$. With the increase of the proportion of Al_2O_3 , the radius of the high-frequency circular arcs was larger. With the increase proportion of Fe_2O_3 , the resistance of the sintered pellets was smaller. And the ability to obtain electrons was stronger and sinter was easier to be reduced. Combined with the phase of these pellets, the appearance of calcium aluminate prevented calcium ferrite from obtaining electrons, leading to the replacement of calcium aluminate with the poor reducibility of sinter.

Generally, the preparation of CFA required CaO and Fe_2O_3 to react at a low temperature to produce calcium ferrite. The crystal shape of calcium ferrite was mainly chunk and pellet. Calcium ferrite crystal had a fast crystallization speed and strong crystallization ability, was closely connected with Fe_2O_3 , and the pellet formed a stable sintering skeleton in the microstructure. When the temperature reached above $1100\text{ }^\circ\text{C}$, the calcium ferrite reached the melting point and melt into Fe_2O_3 to achieve liquid-phase sintering. $CaAl_2O_4$ or Al_2O_3 was easy to dissolve into calcium ferrite to form CFA [21]. It was noted that the amount of Al_2O_3 had an important influence on the sintering process. An appropriate amount of Al_2O_3 improved the wettability and reducibility of the melt during liquid phase sintering [22–24], whereas excessive Al_2O_3 reduced the strength of the sinter and deteriorated the mineral structure. This statement was consistent with the results. It can be seen from Figure 2 that the content of Al_2O_3 was too high, and the competition between Al_2O_3 and Fe_2O_3 to capture CaO affected the formation of calcium ferrite. It showed that most of the CaO was used to form $CaAl_2O_4$ before reaching the CFA generation temperature, resulting in little calcium ferrite. Therefore, the content of Al_2O_3 should be reasonably controlled, so that the sintering system generates more calcium ferrite and less $CaAl_2O_4$ at

low temperatures. When the solid Al_2O_3 or CaAl_2O_4 entered liquid calcium ferrite at high temperatures, it reduces the melting point of calcium ferrite and stabilizes its formation [25].

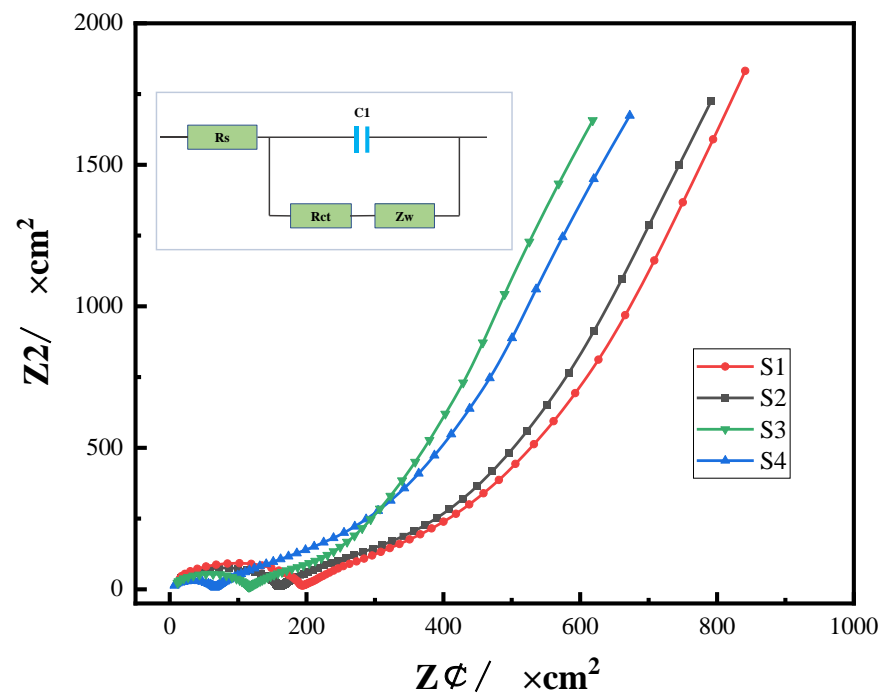


Figure 7. EIS image of samples S1–S4.

4. Conclusions

In this paper, the effect of Al_2O_3 content on the preparation process of CFA was studied by using $\text{CaO-Fe}_2\text{O}_3\text{-Al}_2\text{O}_3$ as raw materials. With the decrease of Al_2O_3 content, CaO was more inclined to combine with Fe_2O_3 to form calcium ferrite. When the Al_2O_3 content was higher, CaO was more inclined to combine with Al_2O_3 to form CaAl_2O_4 . The simultaneous presence of $\text{Ca}_2\text{Fe}_2\text{O}_5$ and CaAl_2O_4 was detected with same content of Al_2O_3 and Fe_2O_3 . After sintering, a stable sintering skeleton was formed. Calcium ferrite was distributed between different particles in chunks or pellets, whereas calcium aluminate was attached to the Al_2O_3 particle. The structure of samples containing more Fe_2O_3 were more compact. Due to the calcium ferrite generated by sintering being evenly distributed in the whole sample, it strengthened the connection between particles. A large amount of calcium aluminate brought by a high Al_2O_3 ratio significantly reduced the reducibility of sinter. The preparation of CFA required the formation of a considerable amount of calcium ferrite during the heating stage. It ensured that other elements were dissolved in calcium ferrite at high temperatures. The formation of calcium ferrite was hindered if there was more Al_2O_3 . Therefore, in order to prepare CFA, it is necessary to control the proportion of raw materials to avoid the formation of calcium aluminate during the heating process, and made Al_2O_3 or calcium aluminate play a beneficial role at high temperatures.

Author Contributions: Z.J. and X.X. designed the experiments; H.Y. wrote the paper; J.M. analyzed the data; X.Q., H.L. and J.L. guided the experiment. All authors have read and agreed to the published version of the manuscript.

Funding: This research was funded by the National Natural Science Foundation of China, grant number 51874141. This research was funded by Hebei Province High-level Talent Funding Project, grant number B2022005007. This research was funded by Tangshan science and technology innovation team training plan project, grant number 21130207D.

Institutional Review Board Statement: Not applicable for studies not involving humans or animals.

Informed Consent Statement: Not applicable for studies not involving humans.

Data Availability Statement: Not applicable.

Acknowledgments: This work was supported by the National Natural Science Foundation of China (No. 51874141), Hebei Province High-level Talent Funding Project (No. B2022005007) and Tangshan science and technology innovation team training plan project (No. 21130207D).

Conflicts of Interest: The authors declare they have no conflict of interest. The funders had no role in the design of the study; in the collection, analysis or interpretation of data; in the writing of the manuscript or in the decision to publish the results.

References

1. Sun, W.; Wang, Q.; Zhou, Y.; Wu, J. Material and energy flows of the iron and steel industry: Status quo, challenges and perspectives. *Appl. Energy* **2020**, *268*, 114946. [[CrossRef](#)]
2. Fernández-González, D.; Ruiz-Bustanza, I.; Mochón, J.; González-Gasca, C.; Verdeja, L.F. Iron ore sintering: Process. *Miner. Process. Extr. Metall. Rev.* **2017**, *38*, 215–227. [[CrossRef](#)]
3. Renard, C.; Liang, Q.B. Study on the calcium ferrite system and its difference of reduction property. *Sinter. Pelletiz.* **1993**, *18*, 36.
4. Mastuno, F.; Harada, T. Changes of Mineral Phases during the Sintering of Iron Ore-Lime Stone Systems. *J. Trans. Iron. Steel. Inst. Jpn.* **1981**, *21*, 318–325.
5. Chen, J.; Cheng, S.; Shevchenko, M.; Hayes, P.C.; Jake, E. Investigation of the Thermodynamic Stability of C(A, F)₃ Solid Solution in the FeO-Fe₂O₃-CaO-Al₂O₃ System and SFCA Phase in the FeO-Fe₂O₃-CaO-SiO₂-Al₂O₃ System. *J. Metall. Mater. Trans. B* **2021**, *52*, 517–527. [[CrossRef](#)]
6. Webster, N.A.; Pownceby, M.I.; Madsen, I.C.; Studer, A.J.; Manuel, J.R.; Kimpton, J.A. Fundamentals of Silico-Ferrite of Calcium and Aluminum (SFCA) and SFCA-I Iron Ore Sinter Bonding Phase Formation: Effects of CaO:SiO₂ Ratio. *J. Metall. Mater. Trans. B* **2014**, *45*, 2097–2105. [[CrossRef](#)]
7. Webster, N.A.; Pownceby, M.I.; Madsen, I.C.; Kimpton, J.A. Effect of Oxygen Partial Pressure on the Formation Mechanisms of Complex Ca-rich Ferrites. *ISIJ Int.* **2013**, *53*, 774–781. [[CrossRef](#)]
8. Webster, N.A.; Pownceby, M.I.; Madsen, I.C. In situ X-ray Diffraction Investigation of the Formation Mechanisms of Silico-Ferrite of Calcium and Aluminium-I-type (SFCA-I-type) Complex Calcium Ferrites. *ISIJ. Int.* **2013**, *53*, 1334–1340. [[CrossRef](#)]
9. Patrick, T.R.; Pownceby, M.I. Stability of silico-ferrite of calcium and aluminum (SFCA) in air-solid solution limits between 1240 °C and 1390 °C and phase relationships within the Fe₂O₃-CaO-Al₂O₃-SiO₂ (FCAS) system. *J. Metall. Mater. Trans. B* **2002**, *33*, 79–89. [[CrossRef](#)]
10. Webster, N.A.; Pownceby, M.I.; Madsen, I.C.; Kimpton, J.A. Silico-ferrite of calcium and aluminum(SFCA) iron ore sinter bonding phases: New insights into their formation during heating and cooling. *J. Metall. Mater. Trans. B* **2012**, *43*, 1344–1357. [[CrossRef](#)]
11. Hessian, M.M.; Kashiwaya, Y.; Ishii, K.; Nasr, M.I.; El-Geassy, A.A. Sintering and heating reduction processes of alumina containing iron ore samples. *Ironmak. Steelmak.* **2008**, *35*, 191–204. [[CrossRef](#)]
12. Machida, S.; Nushiro, K.; Ichikawa, K.; Noda, H.; Sakai, H. Experimental evaluation of chemical composition and viscosity of melts during iron ore sintering. *ISIJ. Int.* **2005**, *45*, 513–521. [[CrossRef](#)]
13. Ahsan, S.N.; Mukherjee, T.; Whiteman, J.A. Structure of fluxed sinter. *Ironmak. Steelmak.* **1983**, *10*, 54–64.
14. Hsieh, L.; Whiteman, J. Effect of oxygen potential on mineral formation in lime-fluxed iron ore sinter. *ISIJ. Int.* **1989**, *29*, 625–634. [[CrossRef](#)]
15. Mochón, J.; Cores, A.; Verdeja, L.F.; Garcia-Carcedo, F. Iron ore sintering part 2. quality indices and productivity. *Dyna* **2014**, *81*, 168–177. [[CrossRef](#)]
16. Pan, J.; Ma, W.Z.; Zhu, D.Q.; Dong, T.; Guo, Z.Q.; Yang, C.C. Effect of Al₂O₃ on sintering, pelletizing and blast furnace smelting. *J. Iron. Steel. Res.* **2021**, *33*, 1095–1108.
17. Ding, X.; Guo, X.M. Effect of Al₂O₃-Doping on crystal structure of α -Fe₂O₃. *J. Chin. Soc. Rare. Earths* **2012**, *30*, 283–286.
18. Hu, C.Q.; Han, T.; Shi, X.F. Formation behavior of calcium ferrite containing aluminum. *Chin. J. Iron. Steel.* **2020**, *55*, 76–80.
19. Wang, M.D. Discrimination between the law of mass action and the concept of elementary reaction. *Chin. J. Univ. Chem.* **2011**, *26*, 81–84.
20. Mirhashemi, S.; Baharvandi, H.R.; Abdizadeh, H.; Ehsani, N. Effects of processing temperature and fabrication method on microstructure and density of multilayer Al₂O₃-ZrO₂ nanocomposites. *Int. J. Mod. Phys. B* **2008**, *22*, 3254–3260. [[CrossRef](#)]
21. Hu, C.Q.; Yang, J.T.; Zhao, K.; Yan, L.G. Effect of Al₂O₃ on the formation mechanism of calcium ferrite. *Chin. J. Iron. Steel. Vanadium Titan.* **2018**, *4*, 109–113.
22. Kalenga, M.K.; Garbers-Craig, A.M. Investigation into how the magnesia, silica, and alumina contents of iron ore sinter influence its mineralogy and properties. *J. S. Afr. Inst. Min. Metall.* **2010**, *110*, 447–456.
23. Umadevi, T.; Prakash, S.; Bandothyay, U.K.; Mahapatra, P.C.; Prabhu, M.; Ranjan, M. Influence of Alumina on Iron Ore Sinter Quality and Productivity. *J. World. Iron. Steel* **2010**, *10*, 12–18.
24. Scarlett, N.V.; Pownceby, M.I.; Madsen, I.C.; Christensen, A.N. Reaction sequences in the formation of silico-ferrites of calcium and aluminum in iron ore sinter. *J. Metall. Mater. Trans. B* **2004**, *35*, 929–936. [[CrossRef](#)]
25. Scarlett, N.V.Y.; Madsen, I.C.; Pownceby, M.I.; Chirstensen, A.N. In Situ X-ray Diffraction Analysis of Iron Ore Sinter Phases. *J. J. Appl. Crystallogr.* **2004**, *37*, 362–368. [[CrossRef](#)]